World Journal of Engineering Research
Print ISSN: 2959-9865
Online ISSN: 2959-9873
DOI: https://doi.org/10.61784/wjer3114

SYSTEMATIC ANALYSIS OF DOMINANT FACTORS CONTROLLING PHOTONIC NANOJET PERFORMANCE FOR SUBSTRATE-EMBEDDED HIGH-REFRACTIVE-INDEX MICROSPHERES

HaoRun Li
School of Physics and New Energy, Chongqing University of Technology, Chongqing 400054, China.

Abstract: Addressing the physical bottleneck that high-refractive-index materials struggle to overcome whispering-gallery modes (WGMs), this study systematically investigated the optical field evolution laws of silicon-based high-refractive-index microspheres in the 1550 nm band, evaluating the influence of four dimensions: environmental refractive index, substrate coupling, asymmetric substrate dimensions, and microsphere embedding depth. Research indicates that elevating the environmental refractive index to above 2.40 can effectively overcome the "focal retraction" phenomenon induced by extreme refractive index contrast. However, in practical on-chip integration applications, the introduction of the underlying substrate triggers a pronounced "substrate dragging effect," leading to massive optical field energy dissipation and focal length degradation. Consequently, the microsphere must maintain a shallow embedding (depth less than 0.08 times the microsphere diameter) to sustain a far-field propagating state; simultaneously, asymmetric substrate dimensions exert a significant anisotropic influence on beam focusing. By constructing a global parameter phase diagram, this study identifies the optimal comprehensive optimization interval, providing engineering recommendations for the on-chip integration and structural design of high-refractive-index infrared micro/nano-detectors.
Keywords: Photonic nanojet; High-refractive-index microsphere; Substrate dragging effect; Mie resonance

1 INTRODUCTION

Infrared photodetector technology, as a core pillar of modern photonics, optoelectronics, and quantum information sensing, plays an irreplaceable role in critical and strategic fields such as precision environmental monitoring, biomedical imaging, space remote sensing, and national security. Its technological evolution is continuously approaching the rigorous physical limits of size, weight, and power [1]. In recent years, with the rapid evolution of autonomous driving and intelligent sensing technologies, automotive light detection and ranging (LiDAR) systems have shown an increasingly urgent demand for high-performance infrared detectors. In practical far-field detection scenarios, the wavefront of the reflected signal arriving at the automotive radar receiver can be approximated as a plane wave, and the system typically requires hundred-meter-range detection and sub-degree angular resolution under complex background interference [2]. However, when the physical pixel size of infrared focal plane arrays gradually shrinks to the micron or even sub-micron scale, the effective absorption cross-section for the interaction between the detector and the optical field drastically reduces, limited by the wave diffraction limit of classical electromagnetic waves. This sharp decline in near-field energy capture capability leads to a severe deterioration of the system's quantum efficiency and responsivity, becoming the underlying physical bottleneck that restricts performance breakthroughs in infrared photodetectors [3].

Among various mesoscopic optical field manipulation mechanisms designed to overcome the diffraction limit, the photonic nanojet (PNJ) has attracted considerable academic attention in recent years as a non-resonant, non-evanescent, and highly efficient spatially localized beam. In 2004, Chen et al. first demonstrated through finite-difference time-domain (FDTD) full-wave simulations that a PNJ can be generated on the shadow side of a specific microparticle under plane-wave illumination, producing a narrow beam characterized by high intensity, low divergence, and a waist width well below the Abbe diffraction limit ($\approx\lambda/2$) [4]. Chinese researchers have also verified that the full width at half maximum (FWHM) of PNJ can stably surpass the diffraction limit, maintaining high-intensity jet propagation over long distances under specific dielectric distributions [5]. Subsequent studies have confirmed that the ultimate capability of microsphere super-resolution imaging is strictly governed by the PNJ waist width, demonstrating immense engineering value in frontier fields such as optical energy focusing and Raman signal enhancement [6]. From the perspective of the physical correlation between focusing and resolution, a narrower nanojet generated by the microsphere combined with a longer longitudinal propagation length yields superior capture of near-field evanescent waves and enhanced super-resolution performance [7]. For infrared detection systems operating in the standard 1550 nm communication band, integrating the super-resolution sub-wavelength focusing characteristics of PNJs into the detector array holds the promise of significantly improving the effective capture rate of incident photons. Concurrently, leveraging its exceptionally low divergence angle can effectively decouple the transverse electromagnetic interactions between pixels in high-density arrays, thereby suppressing optical crosstalk [8].

Although PNJ technology holds immense promise in micro/nano-optics, extending its application to the infrared band and on-chip optoelectronic integration systems reveals that existing theoretical frameworks still face practical challenges

imposed by the dual constraints of material properties and engineering interfaces. According to the classical generalized Lorenz-Mie theory, the prerequisite for a dielectric microparticle to generate a PNJ in external space is that its relative refractive index ratio ($n_{ratio}=n_{particle}/n_{env}$) must be strictly less than 2 [9]. However, the vast majority of early studies were confined to low-refractive-index materials. Silicon (Si), as the mainstay of the optoelectronics industry, exhibits excellent transmittance in the 1550 nm band and is supported by a highly mature CMOS processing platform; nevertheless, its intrinsic refractive index is as high as n≈3.47. This extreme jump in dielectric constant causes a drastic drop in the phase velocity of the incident electromagnetic wave at the illuminated surface, leading to severe curling of the equiphase surfaces within the microsphere. Furthermore, multipole resonance mismatch induces an imaginary distortion of the wave vector at the dielectric interface, forcing the internal reflection angle of the light wave to exceed the critical angle for total internal reflection [10]. This excessive lens focusing effect forces the beam's focal point to regress sharply inward—triggering the fatal "focus retraction" phenomenon [11]. The high-frequency light waves trapped inside are highly susceptible to exciting whispering-gallery modes (WGMs) and can even induce non-negligible nonlinear optical field localization under strong electric fields, ultimately resulting in the complete absence of usable near-field nanojets in the external space.

To break the inherent physical constraints of "focus retraction" in high-refractive-index materials, some previous researchers have attempted to reshape the optical path by etching hemispherical structures [12] or designing complex double-layer core-shell heterostructures [13]. However, hemispherical structures lose the omnidirectional light collection and resonant symmetry of a complete sphere, while complex 3D processing faces the challenge of being incompatible with planar CMOS technology. While ensuring high processing yields, introducing index-matching packaging media (such as highly transparent chalcogenide glasses with tunable refractive indices or specific infrared polymers) to reduce the overall refractive index contrast of the system is the most direct and practically viable dispersion manipulation strategy to successfully "pull" the focus out of the sphere's surface. Furthermore, the vast majority of existing theoretical studies deviate from the engineering reality of infrared focal plane arrays, overlooking the fact that high-refractive-index microspheres must be integrated onto a mechanical substrate. In practical on-chip integration systems, the substrate completely breaks the three-dimensional rotational symmetry of the system along the optical axis. This alteration in the near-field interfacial momentum matching conditions causes the evanescent waves—which would normally propagate along the dielectric boundary—to be extensively "siphoned" into the depths of the substrate as non-radiative leaky modes via Fabry-Perot interference mechanisms and frustrated total internal reflection, thereby triggering a "parasitic dragging effect." Simultaneously, the asymmetric electromagnetic response at the spatial truncation edges leads to severe topological distortion of the wavefront, a phenomenon that shares a homologous physical mechanism with the "photonic hook" observed in Janus symmetry-broken microstructures in recent years [14]. Currently, systematic and quantitative research on the evolutionary characteristics of PNJs in high-refractive-index infrared microspheres under the dual coupling of multidimensional substrate constraints and environmental dispersion matching remains unexplored.

In light of this, this study focuses on the geometric optical characteristics of high-refractive-index silicon microspheres (n=3.47) in the 1550 nm infrared band. It aims to elucidate the synergistic modulation laws of environmental refractive index regulation, three-dimensional asymmetric substrate constraints, and embedding depth on the optical field characteristics of the infrared PNJ. Based on the above analysis, the feasible parameter intervals for high-refractive-index media to overcome focal retraction are provided.

2 PHYSICAL MODEL AND NUMERICAL METHODS

In this study, three-dimensional finite-difference time-domain (FDTD) full-wave numerical simulations are employed to investigate the optical scattering and PNJ evolution characteristics of silicon microspheres and their integrated substrates. A plane wave with a central wavelength of 1550 nm (TM-polarized along the Y-axis) is utilized as the illumination source, incident normally along the positive X-axis. This plane wave closely approximates the physical characteristics of the reflected optical wavefront in far-field automotive LiDAR detection [15]. The standard "Si (Silicon)-Palik" dispersion model is applied to both the microsphere and the substrate materials.

The geometric dimensions of the model are normalized to the microsphere diameter D. Considering the topological proportions of infrared focal plane arrays and CMOS fabrication processes [16], the transverse and longitudinal spans, thickness, and embedding depth of the substrate are initially set to 1.0D, 0.25D, and 0.02D, respectively. This configuration realistically simulates the physical settling morphology encountered in micro/nano-fabrication processes such as spin-coating encapsulation. Regarding boundary conditions and mesh generation, the simulation region is surrounded by an 8-layer perfectly matched layer (PML) to absorb scattered waves, and a symmetric boundary condition is imposed at the minimum boundary of the Z-axis to reduce the computational memory requirement by half [17].

In optical field manipulation systems utilizing high-refractive-index media, achieving effective PNJ output is consistently hampered by stringent physical limitations. To establish the logical foundation of this research and intuitively demonstrate the profound impact of practical engineering constraints on optical field evolution, this section systematically evaluates the steady-state electric field distribution characteristics of silicon microspheres (n=3.47) under three typical physical structural conditions, as shown in Figure 1.

As the physical baseline of this research, we first quantify the intrinsic limitations imposed by a conventional free-space environment on the focusing characteristics of high-refractive-index materials. As illustrated in Figure 1(a), when an intact silicon microsphere is placed in a vacuum or air (n_{env}=1.0), the high-intensity focal point of the incident plane wave passing through the microsphere is entirely confined within the physical boundary of its shadow side. It fails to project

into the external free space, giving rise to focus retraction and whispering-gallery mode phenomena. Examined from the perspective of mesoscopic electromagnetics, this originates from the extreme interfacial impedance mismatch between silicon and air. The excessive refractive index contrast induces severe deflection of the incident light rays at the illuminated surface, forcing the focus to regress sharply inward, thereby producing a severe "focus retraction" effect. The high-frequency light waves trapped inside the microsphere are highly susceptible to total internal reflection at the inner wall, which in turn excites localized whispering-gallery modes. This conclusively demonstrates that without environmental dispersion manipulation, relying solely on high-refractive-index microspheres completely nullifies their value for engineering detection applications.

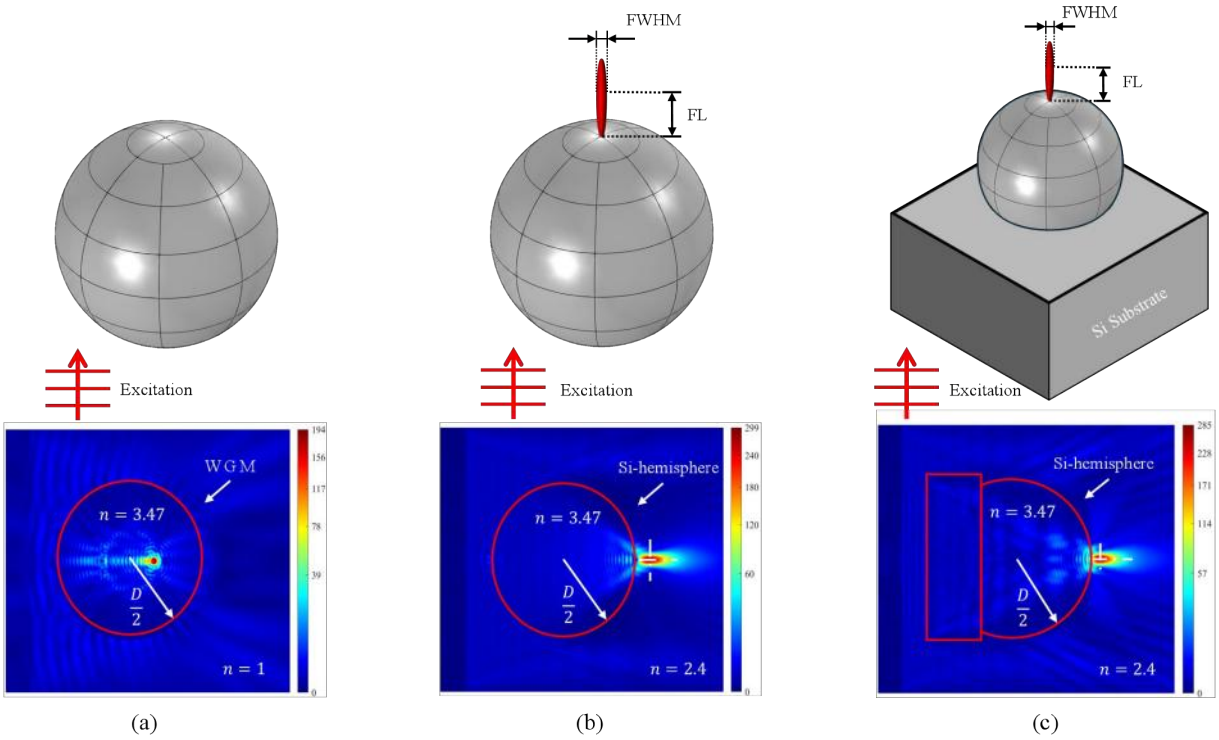

Figure 1 Three-Dimensional Model Configurations and Corresponding FDTD Steady-State Optical Field Evolution of High-Refractive-Index Silicon Microspheres under Different Environmental And Boundary Conditions

To successfully "pull" the focus out of the sphere's surface, the extreme phase jump at the interface must be overcome. This study introduces environmental refractive index matching engineering; as depicted in Figure 1(b), a PNJ is successfully emitted under a high environmental refractive index condition. It is worth noting that in practical infrared optical packaging, the utilization of highly transparent chalcogenide glasses (such as As_2S_3 or As_2Se_3) or customized high-refractive-index infrared polymers can readily provide an environmental refractive index of 2.4 or even higher in the 1550 nm band. By setting n_{env}=2.4, the elevation of the environmental refractive index effectively reduces the relative refractive index contrast of the system (n_{ratio}<2), enabling the originally retracted focus to successfully escape the sphere. Extraction of the steady-state electric field data reveals that the central peak electric field intensity ($|E|^2/|E_0|^2$) of the PNJ surges to 299, demonstrating the remarkable potential of silicon-based materials for super-resolution field localization.
However, the suspended state depicted in Figure 1(b) does not exist in practical on-chip LiDAR integration scenarios; micro/nano-optical components must be immobilized on an underlying mechanical substrate. As illustrated in Figure 1(c), upon introducing the physical constraints of a realistic silicon substrate, even within the same index-matched environment (n_{env}=2.4), the optical field morphology of the PNJ experiences significant degradation: the central peak optical intensity decays to 285, and an asymmetric downward diverging tail emerges at the bottom of the microsphere. This paper, for the first time, defines this mesoscopic optical loss mechanism as the "parasitic substrate dragging effect." Because the underlying substrate is also composed of high-refractive-index silicon, it breaks the spatial rotational symmetry of the system along the optical axis. Consequently, it "forcibly drags" the near-field evanescent waves that would normally propagate along the microsphere surface, causing them to leak deep into the substrate in the form of non-radiative leaky modes.

3 THE INFLUENCE OF SILICON SUBSTRATE ON PNJ

Driven by the practical engineering requirements of high-density infrared optoelectronic integration, the generation environment of PNJs inevitably transitions from an ideal suspended state to a complex on-chip integration space. Conventional mesoscopic scattering theories often overlook the fundamental disruption of electromagnetic boundary conditions caused by the underlying supporting substrate. By introducing a high-refractive-index silicon substrate, this

section thoroughly reveals the evolutionary characteristics of PNJs subjected to this underlying physical barrier from the dual perspectives of macroscopic propagation phase and near-field energy conservation.

To quantitatively evaluate the physical pulling effect of the substrate configuration on the beam propagation path and energy distribution, this section conducts a comprehensive analysis by jointly extracting the evolutionary trends of the system's steady-state focal length and the transverse electric field at the focal plane.

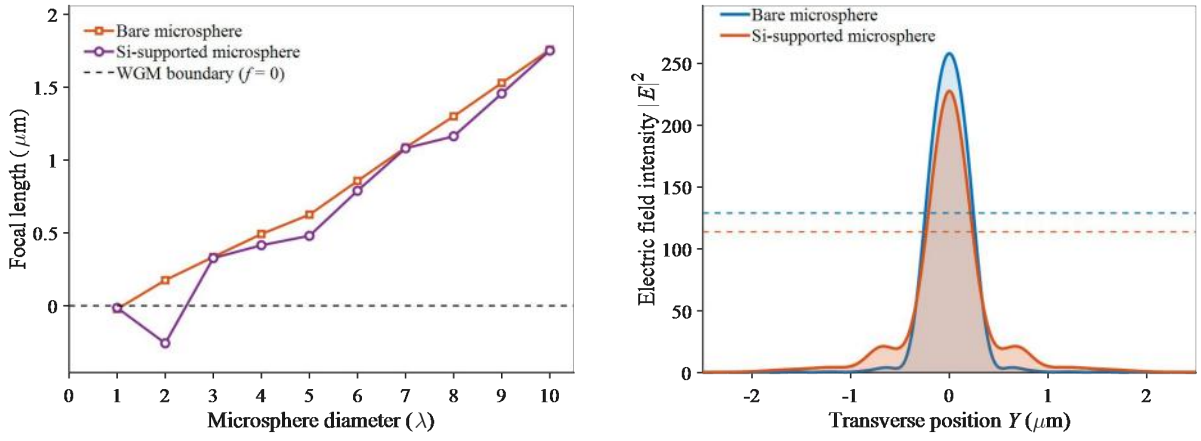

(a) (b)

Figure 2 Comprehensive Clamping Effect of Substrate Constraints on the Macroscopic Evolution and Microscopic Energy Distribution of PNJs under Environmental Refractive Index Matching

A detailed observation of Figure 2(a) reveals that in the larger-scale regime (D>3 λ), the focal lengths of both models exhibit a step-like increase extending toward the far field as the microsphere diameter increases. Within the framework of geometrical optics, this can be attributed to the increased equivalent radius of curvature at the illuminated surface of the microparticle, which reduces the numerical aperture and thereby suppresses the inward focusing induced by spherical aberration. However, in the small-scale limit regime ranging from sub-wavelength to near-wavelength dimensions (e.g., D≤2 λ), an abrupt physical transition occurs: while the ideal suspended microsphere (orange line) maintains its ability to project a focus outward, the focal length of the substrate-integrated microsphere (purple line) experiences a highly destructive, precipitous drop, plunging directly into the f≤0 regime (where the focus retracts into the interior or onto the surface of the sphere).

This anomalous evolution and extreme size sensitivity fundamentally arise because the introduction of the high-reflectivity substrate reshapes the simple “lens focusing” system into a miniature Fabry-Perot resonator. Consequently, the far-field wave emitted from the microsphere and the back-reflected wave from the substrate surface must satisfy a stringent phase resonance condition:

$$\Delta\Phi=\frac{4\pi n_{\text{eff}}D_{\text{eff}}}{\lambda}\cos\theta+\Delta\phi_{\text{interface}}, \tag{1}$$

where n_{eff} is the equivalent environmental refractive index, D_{eff} is associated with the longitudinal geometric dimension of the microsphere, and $\Delta\phi_{\text{interface}}$ denotes the additional phase shift introduced by the high-refractive-index interface. With the continuous sweeping of the microsphere diameter D, the optical path difference within the resonator periodically traverses constructive and destructive interference conditions, causing the focal length curve to deviate from pure linearity. Particularly in the small-scale limit, the drastic alteration of near-field momentum matching conditions induced by the substrate disrupts the total internal reflection at the inner wall of the sphere, resulting in a significant amplification of the excitation cross-section for whispering-gallery modes (WGMs) [18]. The electromagnetic energy, originally at the critical threshold of escaping, is forcibly confined back into the interior, which macroscopically manifests as a “dragging plunge” in the focal length.

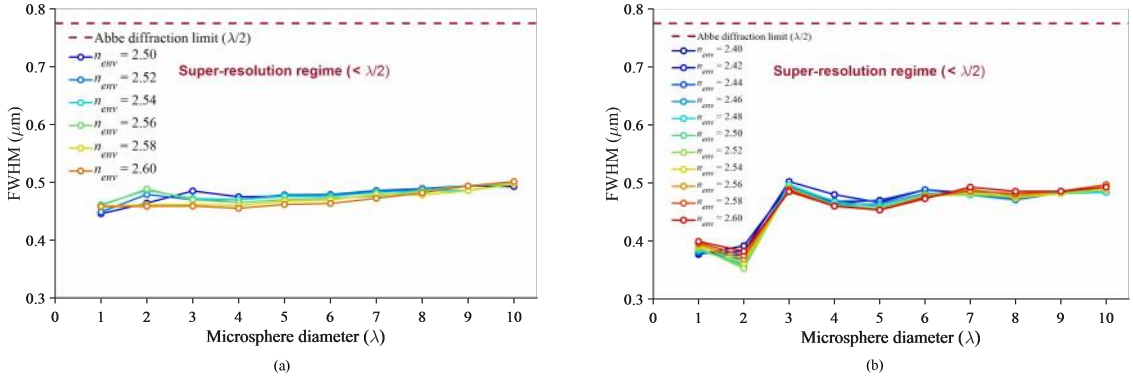

(a) (b)

Figure 3 Comprehensive Evolution and Limit Breakthrough of the Full Width at Half Maximum (FWHM) under Environmental Variable Sweeps

More critically, this substrate constraint not only modulates the phase but also directly depletes the optical field energy of the system. As illustrated in the transverse profile in Figure 2(b), compared to the ideal suspended control group (blue line, peak intensity of approximately 255), the central main peak energy density at the focal point of the substrate-integrated model (orange line) exhibits a significant collapse (decreasing to approximately 228), accompanied by distinct broadening of the side lobes. In its physical essence, this degradation mechanism corresponds to frustrated total internal reflection (FTIR) and the non-radiative leaky mode tunneling siphon effect induced by the high-refractive-index silicon substrate [19]. This paper defines this degradation mechanism as the "parasitic substrate dragging effect." This shares a homologous mechanism with the near-field energy redistribution phenomenon observed by Chinese researchers investigating the coupling between microspheres and underlying substrates (such as metallic or plasmonic structures): the substrate, acting as a strongly asymmetric spatial boundary, inevitably induces plasmonic coupling or non-radiative leaky modes, thereby directly siphoning the focused optical field energy from the microsphere [20]. In the dimension of energy transport, the tightly bonded high-refractive-index silicon substrate (n_{si}=3.47) completely breaches the electromagnetic potential barrier at the bottom of the microsphere. A substantial portion of the evanescent wave components, which would otherwise propagate along the dielectric boundary and converge at the far-field focal plane, are "siphoned" deep into the substrate as non-radiative leaky modes. This triggers a direct and irreversible dissipation of the Poynting vector energy flux in the primary focal region. Simultaneously, the broken symmetry leads to a splitting of the optical integration paths between the upper and lower hemispheres. The resulting disorder in the wavefront phase forces a fraction of the photon energy to be displaced into higher-order side lobes, further deteriorating the central energy convergence.

As a core metric for quantifying the degree of transverse optical field localization and the level of pixel crosstalk isolation, the full width at half maximum (FWHM) exhibits even more extreme sensitivity to perturbations in microscopic boundary conditions. Analysis of Figure 3(a) indicates that, after excluding the early mode-transition region, the FWHM of the ideal suspended microsphere exhibits a smooth, gentle, and monotonically broadening trend with increasing dimension D. Physically, this maps the smooth transition of the optical focusing mechanism from mesoscopic resonance to the classical paraxial optical approximation. In stark physical contrast, Figure 3(b), which incorporates the integrated substrate, displays violently fluctuating "V-shaped" depressions and nonlinear oscillatory characteristics across the entire size domain. The underlying physical root of this phenomenon is not generalized Mie scattering; rather, the high-refractive-index substrate acts as a strongly asymmetric external spatial potential field, forcibly lifting the rotational degeneracy of the higher-order electric and magnetic dipoles excited within the microsphere [21].

The lifting of this degeneracy not only severely distorts the nodal line distribution of the three-dimensional standing waves within the microsphere but also induces periodic disorder and redistribution in the relative phase differences of the transmitted multipole waves of various orders during their spatial interference superposition on the shadow side. Particularly within the critical resonant size regime of D=1~ 2 λ multipole modes of specific orders experience profound transverse destructive interference. This finely "sculpts" the transverse energy envelope of the electromagnetic wave, consequently causing the FWHM to plummet to a deep-subwavelength minimum of approximately 0.35 μm. Although the interference patterns exhibit drastic fluctuations with varying dimensions, under the index-matched environment of n_{env}≥2.40, the FWHMs of all PNJs are firmly clamped below the Abbe diffraction limit (the red line in Figure 3, λ/2≈0.775 μm). This quantitative result conclusively demonstrates that harnessing multipole interference reorganization through precise dimensional optimization is an effective engineering approach to overcome the bottleneck of infrared pixel crosstalk.

4 THE INFLUENCE OF SUBSTRATE EMBEDDING DEPTH ON PNJ

In the preceding section, this study verified the modulation effect of the substrate on the far-field wavefront phase and near-field energy flux based on fundamental electromagnetic mechanisms. However, in the monolithic integration manufacturing of practical on-chip micro-electromechanical systems or high-density infrared photodetector arrays, micro/nano-dielectric spheres are not simply suspended above the substrate via an ideal geometric "point contact." To ensure the structural stability and interfacial phonon conduction efficiency of the devices under severe thermo-mechanical stress, microstructures typically need to be partially subsided and embedded into the underlying medium through specific wafer-scale micro/nano-fabrication processes (such as polymer spin-coating and curing, isotropic chemical etching, or thermal reflow self-assembly). This section advances the physical model from a slightly perturbed boundary to a realistic "surface contact" immobilized morphology, systematically and quantitatively investigating the nonlinear clamping effect of the interfacial embedding depth on the macroscopic evolution trajectory and microscopic localized modes of the PNJ. To evaluate the impact of immobilization deformation on the beam propagation path from the dual perspectives of geometrical and wave optics, this section meticulously extracts the continuous evolution phase diagrams correlating the microsphere's embedding depth into the substrate (0.02 D~0.14 D) with the core characteristic parameters of the PNJ.

As revealed by the macroscopic evolution curve in Figure 4(a), accompanying the continuous deepening of the immobilized interface, the effective focal length of the PNJ fails to maintain a stable, high-tolerance output. Instead, it exhibits a nonlinear retraction characteristic that is exceedingly sensitive to geometric boundaries. Particularly after the embedding depth surpasses the physical threshold of 0.08 D, the focal length experiences a prominent step-like decay, ultimately diminishing to approximately 0.5 μm under the deep-embedding condition of 0.14 D. Examined against the

macroscopic scale of D=5 λ (7.75 μm), this extremely short focal length signifies that the PNJ, which should conventionally extend into the far field, has drastically lost its penetration capability. Consequently, the equivalent focus becomes highly localized near the physical outer shell boundary of the microsphere.

In physical essence, this sharp retraction of the focal length is a geometric phase truncation effect induced by the severe distortion of the optical path difference. As the embedding depth increases, the contact volume between the lower half of the microsphere and the high-refractive-index silicon substrate (n_{Si}=3.47) expands exponentially. Geometrically, this not only deprives the illuminated surface of the microsphere of its effective lens numerical aperture but also causes the phase velocity of the light waves in the lower half to be significantly lower than that in the upper half (environmental medium n_{env}=2.40). This top-bottom asymmetric dielectric distribution disrupts the originally smooth equiphase surfaces, leading to a drastic backward shift of the equivalent center of refraction. Concurrently, the topological expansion of the contact interface opens a substantial non-radiative leakage channel for electromagnetic energy. The abrupt loss of optical propagation momentum ultimately leaves the system spatially incapable of maintaining the emission of a far-field jet.

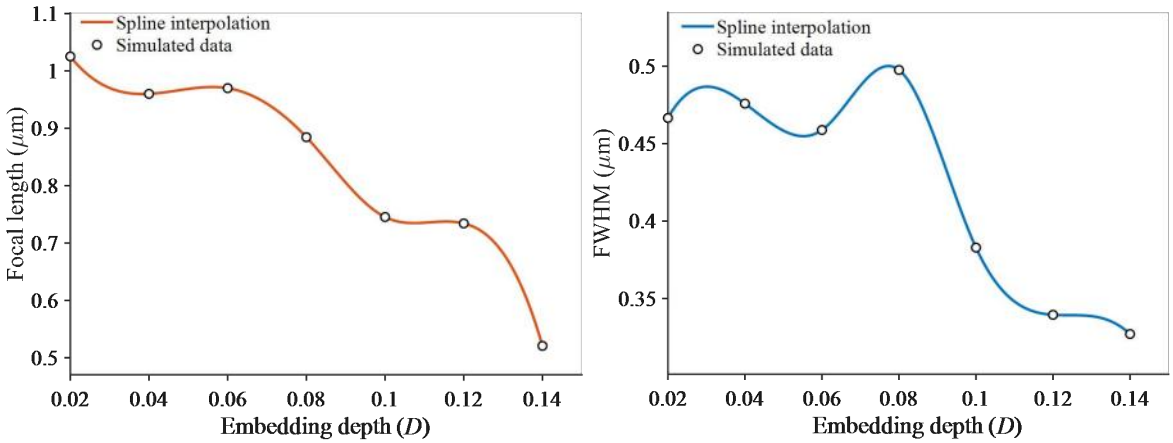

(a) (b)

Figure 4 Nonlinear Clamping Effect and Mode Evolution Mechanism of the Interfacial Immobilized Embedding Depth on the Core Characteristic Parameters of the PNJ

Having established the correlation between phase truncation and focal length degradation, this study further jointly analyzes the FWHM metric, which characterizes the near-field super-resolution capability, as shown in Figure 4(b). During this multidimensional cross-validation process, this research reveals an underlying physical "data trap" that is highly susceptible to misinterpretation during parameter optimization in mesoscopic photonics. As observed from the evolution trajectory in Figure 4(b), within the shallow embedding regime (0.02D~0.08D), the FWHM curve exhibits nonlinear oscillations with a slight broadening tendency, which is highly consistent with the previously discussed mechanism of higher-order multipole phase mismatch. However, when the embedding depth surpasses the critical point and approaches 0.14 D, the FWHM curve experiences a highly anomalous and drastic “shrinkage,” with its value plummeting to approximately 0.33 μm.

Interpreting this phenomenon in isolation, divorced from the focal length parameters in Figure 4(a), can easily lead to the misconception that "deeply embedded high-refractive-index microspheres can achieve ultra-high resolution." However, by rigorously establishing the physical topological correlation between the focal length attenuation and the abrupt waist shrinkage, it can be deduced that this exceedingly small FWHM does not denote a PNJ in a healthy propagating state. Because the focal length closely approaches the microsphere surface at this point, the extremely narrow optical field measured at the focal plane has fundamentally degenerated into near-field surface states or evanescent wave components highly localized at the solid-liquid dielectric interface. The wave vector of such localized fields is purely imaginary in the propagation direction. Although it exhibits extreme transverse narrowing due to the accumulation of interfacial polarization charges, its electromagnetic energy decays exponentially within an exceedingly short distance from the dielectric surface. Consequently, it fails to provide the working depth of focus and longitudinal energy flux transport capability essential for optical engineering applications, signifying a fundamental transition in the physical propagation mode of the PNJ.

The orthogonal degradation phase diagram presented in Figure 4 not only elucidates the mode evolution mechanisms in mesoscopic optics but also provides rigorous engineering guidelines for the physical tape-out of next-generation optoelectronic chips: deep interfacial embedding is the critical limiting factor restricting the evolution and energy coupling of high-refractive-index PNJs.

5 COMPREHENSIVE INFLUENCE OF SUBSTRATE DEPTH AND WIDTH ON PNJ

Having established the necessity of shallow interfacial embedding for maintaining the eigenstate of optical field propagation, this section extends the optimization scope of the physical architecture from longitudinal depth truncation to the transverse on-chip integration plane (Y-Z plane). In the monolithic tape-out design of ultra-large-scale infrared

focal plane arrays, the physical span of the substrate isolation band between adjacent dielectric micro-antennas directly dictates the pixel pitch and the ultimate integration density of the chip. In previous studies, the horizontal and vertical dimensions of the substrate have conventionally been assumed to be perfectly symmetric. In this section, we decouple the horizontal span (Y_{span}) and the vertical span (Z_{span}) of the substrate, treating them as two independent variables to perform cross-sweep simulations. Through comparative experiments with independently varying dimensions, we systematically elucidate how the boundary geometries of the substrate along different directions specifically influence the polarization characteristics of the PNJ. Finally, taking into account diverse practical engineering requirements, we provide specific recommendations for substrate dimension selection directly derived from this dimensional evolution phase diagram.

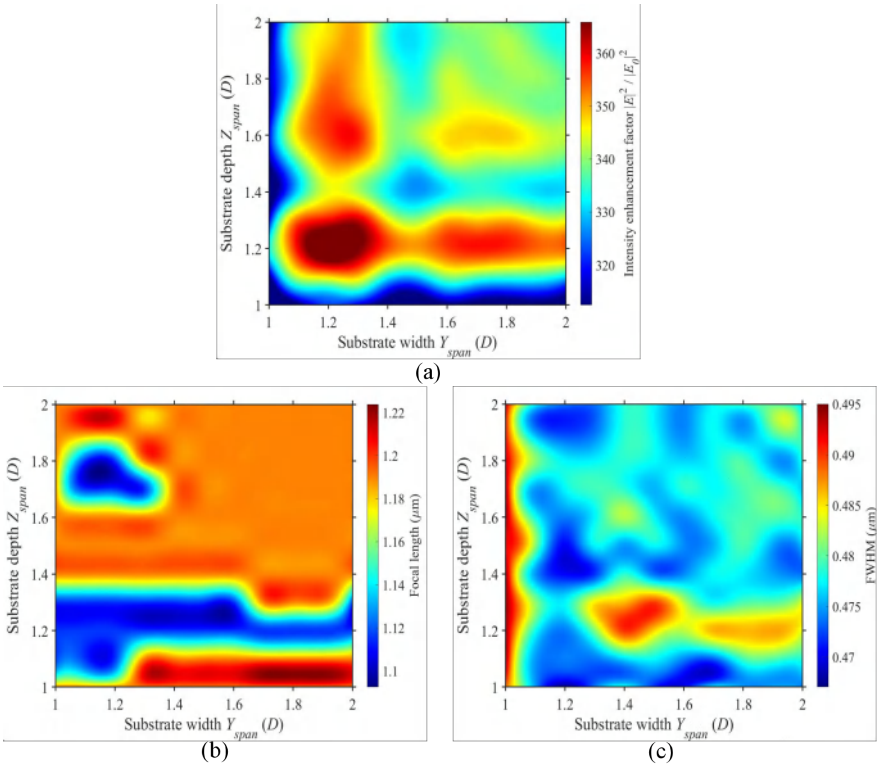

Figure 5 Two-Dimensional Phase Transition Colormaps Illustrating the Continuous Evolution of the Core Electromagnetic Characteristic Parameters of the PNJ with Respect to the Orthogonal Substrate Span under the Baseline Matching Condition

To investigate the dragging weight of asymmetric physical plane dimensions on the equivalent center of refraction from a wave perspective, this section first conducts an in-depth decoding of the topological features of the two-dimensional focal length phase transition colormap shown in Figure 5(b). As can be observed from Figure 5(b), during the process of the proportional expansion of the substrate's biaxial dimensions, the focal length colormap does not exhibit the intuitively expected centrosymmetric concentric-circle gradient topology. Instead, it displays prominent parallel transverse stripe structures aligned parallel to the Y_{span} axis. This nonlinear topological distortion indicates that when the system undergoes spatial perturbations of equal magnitude in the controlled variables, the clamping weight and regulatory efficacy of the vertical span Z_{span} on the system's focal length exhibit absolute dominance over those of the horizontal span Y_{span}. In other words, the topological expansion of the spatial boundary along the Z-axis dramatically modulates the longitudinal focusing position of the beam, whereas boundary variations along the Y-axis have a relatively weak impact on the focal length.

The underlying physical root of this strong anisotropic dynamical response lies in the selective electromagnetic coupling between the transverse magnetic (TM) intrinsic polarization state of the incident plane wave (where its electric field vector $\vec{E}$ is strictly linearly polarized along the Y-axis) and the mesoscopic geometrically truncated edges [22]. According to the Maxwell electromagnetic boundary conditions for continuity, at physical boundaries perpendicular to the direction of electric field polarization (the transverse Y_{span} truncated edges, whose interface normal is along the Y-axis), the spatial electric field manifests as a normal component E_n. Due to the massive dielectric constant jump between the high-refractive-index silicon substrate and the environmental medium ($\varepsilon_{Si}\approx12$ VS $\varepsilon_{env}\approx5.76$), the normal electric field exhibits an extremely discontinuous step distribution across the interface ($\varepsilon_{Si}E_{n,Si}=\varepsilon_{env}E_{n,env}$). This intense accumulation of interfacial polarization charges strongly confines a massive amount of electromagnetic energy within the substrate directly beneath the microsphere, thereby greatly diminishing the scattering cross-section for outward radiation and escape.

Conversely, at physical boundaries parallel to the direction of electric field polarization (the vertical Z_{span} truncated edges, whose interface normal is along the Z-axis), the spatial electric field manifests as a tangential component E_t. Maxwell's equations strictly dictate that the tangential electric field must remain absolutely continuous across the dielectric interface.

This continuity characteristic allows the near-field surface waves and propagating evanescent waves emitted from the microsphere to smoothly penetrate and propagate outward along the Z_{span} boundary, thereby experiencing deep and strong coupling with the spatial truncated edges of the substrate in the Z direction. Consequently, the spatial boundary topology along the Z-axis directly determines the degree of the wavefront phase jump for this portion of the escaping optical flux, macroscopically dominating the backward pull on the equivalent numerical aperture center of the optical field. This discovery implies that in the two-dimensional layout of infrared micro/nano-optoelectronic chips, the polarization direction itself acts as a core lever for breaking electromagnetic boundary symmetry and realizing heterogeneous optical modulation.

When investigating the evolution trajectory of the near-field super-resolution characteristics of the jet, the two-dimensional FWHM phase transition colormap in Figure 5(c) exhibits an optical interference phenomenon distinctly different from the smooth stripes of the focal length. The FWHM phase transition colormap displays a highly discrete, "mottled island-like" distribution resembling complex speckle interference patterns across the entire two-dimensional parameter space. It is particularly worth emphasizing that, although the distribution in the colormap exhibits strong spatial heterogeneity and nonlinear oscillation, the absolute fluctuation window of its global values is stringently compressed within a narrow theoretical bandwidth of 0.470 μm to 0.495 μm. This global maximum (0.495 μm) remains far below the classical Abbe diffraction limit for an infrared 1550 nm light source in the current matched environment ($\lambda/2n_{env}\approx0.323$ μm; 0.775 μm in a full vacuum), conclusively demonstrating that the deep-subwavelength focusing capability of this integrated system possesses extremely high robustness against multidimensional spatial perturbations.

In physical essence, this mottled and minute nonlinear wavefront oscillation is the coherent mapping of mesoscopic-scale edge diffraction effects in the far field [23]. In a realistic on-chip integrated architecture, the four spatial truncated edges of the substrate essentially act as four sets of distributed "secondary scattering line sources." According to the Huygens-Fresnel principle, as the near-field surface waves excited by the incident electromagnetic wave propagate to these physical boundaries, secondary diffracted waves are generated due to the dielectric discontinuity. During the continuous two-dimensional parameter sweep of the substrate's orthogonal spans from 1.0 D to 2.0 D, the absolute geometric optical paths from these four sets of distributed line sources to the central optical axis of the microsphere are continuously modulated. Consequently, upon propagating to the predetermined focal plane, they accumulate different phase factors $\exp(i\vec{k}\cdot\vec{r})$. These faint secondary diffracted waves undergo high-order coherent superposition in space with the high-intensity primary jet excited by the main body of the silicon microsphere. It is precisely this periodic mismatch, alignment, and reorganization of the edge spatial diffraction phase with varying geometric spans that finely "sculpts" the transverse energy envelope of the electromagnetic wave in the focal region, thereby triggering high-frequency spatial jumps in the waist width at the nanoscale, akin to an optical "breathing effect." The establishment of this mechanism sounds an alarm for the manufacturing tolerance design of silicon-based micro/nano-chips: although edge diffraction cannot undermine the baseline of breaking the diffraction limit, designers must recognize that nanoscale perturbations in etching lines will induce minute fluctuations in the waist envelope.

Having elucidated the independent physical mechanisms of anisotropic focal length clamping and high-frequency waist oscillation, determining the final three-dimensional substrate isolation dimensions for practical optoelectronic integrated tape-outs is elevated to a multivariable systems engineering problem. Because there is no single optimal solution in reality that can simultaneously push optical intensity, focal length, and resolution to their absolute extremes, it is necessary to break away from the blind spots of traditional single-parameter optimization. Instead, we must establish a model for "multidimensional modulation and parameter selection for differentiated engineering scenarios" based on two-dimensional panoramic colormaps. By conducting a multi-objective cross-correlation of Figure 5(a), 5(b), and 5(c), customized packaging and tape-out parameter guidance can be provided for high-signal-to-noise-ratio far-field active detection platforms (such as anti-noise systems at the receiving end of automotive LiDAR).

The core objective of such engineering architectures is to extract the ultimate light-collection efficiency of a single pixel, in order to capture faint reflected signals over long distances and under strong background noise (such as intense sunlight, rain, and fog). In this context, designers should assign the primary weight entirely to the electric field intensity enhancement factor shown in Figure 5(a). Joint analysis of the colormaps reveals that at the specific geometric coordinate intersection of $Y_{span}=Z_{span}=1.2\,D$, there exists a dark red "energy resonance hotspot" representing the global absolute maximum, where the local electric field intensity enhancement factor ($|E|^2/|E_0|^2$) achieves a substantial leap. Based on deductions from the higher-order coherence theory of wave optics, 1.2 D is not a numerical coincidence but a "golden resonance ratio" capable of triggering perfect geometric coherent compensation. Under this boundary constraint, when the secondary scattered waves excited by the four edges of the substrate arrive at the focal plane, their accumulated optical path phase achieves exact zero-phase-difference alignment with the central phase of the primary jet, inducing perfect constructive interference. This "geometric coherent compensation" mechanism physically neutralizes and counteracts the "parasitic dragging loss" induced by the high-refractive-index substrate described previously, achieving the ultimate recovery and reconvergence of the energy flux in three-dimensional space. Although under these parameters, the FWHM (approximately 0.475 μm) incurs a broadening cost of a few nanometers compared to the theoretical absolute minimum, this trade-off yields an order-of-magnitude leap in energy flux concentration efficiency. Furthermore, it anchors the system in the most stable anti-perturbation plateau region of the focal length in Figure 5(b), thus rendering it an ideal balanced parameter for the design of infrared pixel arrays such as LiDAR.

6 COMPREHENSIVE INFLUENCE OF ENVIRONMENTAL REFRACTIVE INDEX AND MICROSPHERE RADIUS ON PNJ

Having thoroughly decoupled the perturbation mechanisms of the underlying substrate's local geometric truncation (embedding depth and orthogonal topological span) on the near-field propagation eigenstates, this study has successfully established microscopic design guidelines relying on "geometric coherent compensation" to counteract the parasitic dragging effect. However, to elevate this fundamental physical understanding into a macroscopic engineering blueprint with universal guiding significance for practical infrared on-chip monolithic integration, this section transitions the scope of physical optimization from microscopic geometric parameters to the macroscopic system dimension. It conducts high-density joint scanning and intrinsic phase transition mapping across the two-dimensional full-parameter space constructed by the physical diameter of the microsphere D and the environmental refractive index of the system n_{env}.

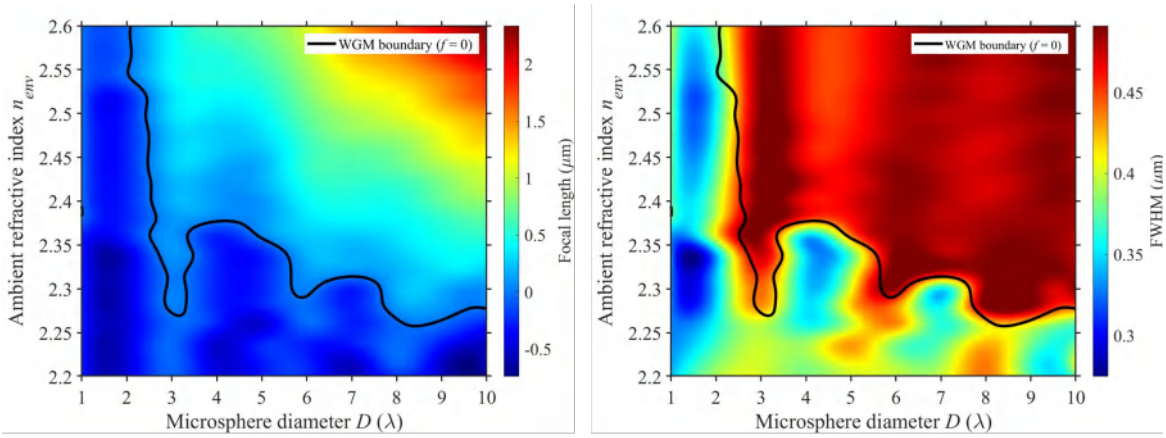

Figure 6 Global Phase Transition Topological Colormaps of the Core Characteristic Parameters of the PNJ within the Macroscopic Two-Dimensional Parameter Space under Silicon Substrate Constraints

When challenging the extreme limits of optical field localization in high-refractive-index media, determining how to fundamentally overcome "focal retraction" and decouple the constraint of the dielectric interface on the optical flux is the primary prerequisite for activating an external jet. According to classical generalized Mie scattering theory, the relative refractive index ratio of the system is defined as:

$$n_{ratio}=\frac{n_{sphere}}{n_{env}}, \tag{2}$$

where n_{ratio} represents the relative refractive index ratio, and n_{sphere} represents the refractive index of the microsphere. The classical theoretical threshold for forming a high-quality external PNJ requires $n_{ratio}<2$.For a high-refractive-index silicon microsphere ($n_{sphere}\approx3.47$) immobilized on a homogeneous silicon substrate, satisfying this refractive index ratio criterion necessitates a substantial enhancement of the dispersive capability of the environmental medium.

As observed from Figure 6(a) and 6(b), the entire vast two-dimensional macroscopic parameter space is clearly partitioned into two major physical realms by a meandering thick black solid line (f=0). The dark blue topological depression region to the left and below this solid line ($f\leq0$) signifies that the optical field energy struggles to radiate outward, and the system is primarily occupied by whispering-gallery modes (WGMs) dominated by total internal reflection or near-field surface states; crossing the restrictive boundary of this black line marks the effective formation of an externally propagating state PNJ carrying a real wave vector. Under the stringent constraints that fully account for complex substrate perturbations, this study quantitatively calibrates the steady-state environmental refractive index threshold for activating the silicon-based external PNJ within the 1550 nm infrared band to be approximately $n_{env}\geq2.40$(corresponding to $n_{ratio}\leq1.44$). This physical criterion provides a clear guiding boundary for the material selection of high-refractive-index passivation layers (such as chalcogenide glass) for next-generation on-chip optoelectronic devices.

Further scrutinizing the geometric morphology of this WGM critical boundary, the research reveals the higher-order mesoscopic electromagnetic nonlinear dynamic evolution process hidden beneath the macroscopic phase diagram. The thick black solid line outlining the boundary in Figure 6 is not a smooth, monotonic asymptote; rather, within the critical dimensional interval of D=2.5 λ~ 4 λ, it exhibits a pronounced "downward depression" and nonlinear topological distortion. Particularly near the coordinate node of D=3 λ, the system demonstrates extremely strong anti-perturbation characteristics, enabling the microsphere to overcome substrate leaky mode losses and successfully emit a complete PNJ outward even under a lower environmental refractive index ($n_{env}\approx2.27$).

This local topological depression profoundly characterizes the hidden "Mie resonance mode hopping" mechanism at the mesoscopic scale [24]. Accompanying the continuous expansion of the microsphere's physical dimension, the order of the electromagnetic eigen-resonances excited within it undergoes discrete transitions. The specific dimension of D=3 λ precisely coincides with an anti-leakage eigen-resonance state constructed by higher-order electromagnetic multipoles. Under this specific coherent superposition mode, the physical immunity of the spatial standing wave network excited

within the microsphere against the parasitic dragging effect of the substrate's bottom surface is significantly enhanced, thereby forming a prominent mode-stability window in the two-dimensional phase diagram.

After successfully crossing the survival threshold of f=0, the core contradiction in the design of on-chip optical antennas shifts to how to ultimately optimize the subwavelength transverse resolution of the beam while ensuring a sufficient working depth of focus (to penetrate underlying passivation or isolation layers). Existing relevant simulation system demonstrations have also pointed out the existence of this multidimensional parameter trade-off: variations in the microsphere's dimension will induce an intertwined response in resolving power and depth of focus (jet length), often necessitating the search for specific resonant states of the microparticle to balance both aspects [25].

An orthogonal comparison of the large-dimension, high-refractive-index regions in the upper right of Figure 6(a) and 6(b) (i.e., the D>6 λ quadrant) exposes a physical reality within the mesoscopic optical system. In the mapping of Figure 6(a), this quadrant presents a broad expanse of red high-value regions, signifying that the focal length has acquired superior far-field extension capability. However, shifting to the same physical quadrant in Figure 6(b), this region manifests as a dark red degradation zone representing FWHM broadening. This topological inversion demonstrates that relying solely on the continuous expansion of geometric scale to achieve a longer focal length will inevitably introduce a multitude of high-spatial-frequency oscillatory modes. These complex higher-order modes are highly susceptible to "spatial decoherence" during far-field interference superposition, leading to a decline in the transverse localized wavefront fidelity of the jet, and ultimately triggering the degradation of near-field super-resolution capabilities.

To balance the mutual constraints between focal length extension and super-resolution localization, this study introduces a global optimization architecture of "multidimensional topological overlay." By performing a two-dimensional spatial matrix intersection mapping between the light blue to cyan transition band in Figure 6(a), where the focal length satisfies the requirements for underlying optoelectronic coupling ("sufficient depth of focus"), and the dark blue phase transition band in Figure 6(b), which characterizes the extreme compression of the waist ("extreme localization"), this research establishes an excellent comprehensive performance stationary point within the global phase diagram: an absolute microsphere diameter of D=3 λ.

By locking onto this core dimension of D=3 λ and matching it with the high process tolerance interval of $n_{env} \in [2.45,2.50]$, the system not only maximizes the utilization of the anti-interfacial-perturbation dividend endowed by "Mie mode hopping," ensuring the robustness of the jet emission state, but also efficiently compresses the waist span of the transverse electromagnetic energy below the theoretical Abbe diffraction limit. This global calibration, based on the macroscopic full-parameter space, provides a micro/nano-topological parameter atlas free from repeated trial and error for infrared LiDAR and high-density InGaAs focal plane detector arrays, demonstrating significant potential for industrial tape-out translation.

7 CONCLUSION

Addressing the fundamental physical bottleneck that high-refractive-index media in infrared optoelectronic detection systems struggle to form effective PNJs, this study systematically investigated the evolution laws of the optical field for silicon-based microspheres in the 1550 nm band under the dual constraints of environmental refractive index matching and on-chip substrates. By constructing a high-precision FDTD numerical model, this paper elucidated the generation mechanisms and modulation pathways of a series of mesoscopic optical effects—such as focal retraction, substrate parasitic dragging, and asymmetric boundary diffraction—during the transition of high-refractive-index microspheres from an ideal suspended state to a realistic integrated state. The research results indicate that the focal retraction and whispering-gallery mode excitation, which are induced by high-refractive-index silicon microspheres in an air environment, can be overcome by elevating the environmental refractive index to above 2.40. Further research demonstrates that the embedding depth of the microsphere into the substrate is a critical process parameter limiting PNJ performance, causing the narrow optical field at the focal plane to degrade into near-field surface states. Regarding the optimization of the substrate's transverse dimensions, this paper reveals a pronounced anisotropic response in focal length modulation by boundaries in different directions, which is induced by the TM polarization state of the incident light. Among these, the substrate span along the direction parallel to the electric field plays a dominant role in beam propagation. By constructing a global parameter phase diagram encompassing the microsphere diameter and the environmental refractive index, this paper quantitatively provides the environmental refractive index threshold for activating the silicon-based external PNJ, and identifies the comprehensive optimization interval of D=3 λ and an environmental refractive index between 2.45 and 2.50. Under these parameters, the system can utilize the Mie resonance mode hopping mechanism to effectively suppress the substrate parasitic dragging effect, while simultaneously compressing the transverse waist width below the Abbe diffraction limit. The aforementioned research conclusions provide clear simulation bases and parameter value recommendations for the structural design of high-refractive-index infrared micro/nano-detectors, holding reference value for promoting the practical application of PNJ technology in on-chip infrared optoelectronic integration systems.

COMPETING INTERESTS

The authors have no relevant financial or non-financial interests to disclose.

REFERENCES

[1] Rogalski A. Recent progress in infrared detector technologies. Infrared Physics & Technology, 2019, 102: 102976.
[2] Steinvall O K. Performance of laser tracking of small targets during turbulence and beam jitter. Proceedings of SPIE, 2003, 5086.
[3] Downs C, Vandervelde T E. Progress in infrared photodetectors since 2000. Sensors, 2013, 13(4): 5054-5098.
[4] Chen Z, Taflove A, Backman V. Photonic nanojet enhancement of backscattering of light by nanoparticles: a potential novel visible-light ultramicroscopy technique. Optics Express, 2004, 12(7): 1214-1220.
[5] Jia R, Yang Z, Pan X, et al. Study on the characteristics of photonic nanojets generated by non-uniformly coated microspheres. Acta Physica Sinica, 2024, 74(9): 094202.
[6] Yang H, Trouillon R, Huszka G, et al. Super-resolution imaging of a dielectric microsphere is governed by the waist of its photonic nanojet. Nano Letters, 2016, 16(8): 4862-4870.
[7] Liu X, Zhou T, Wang J, et al. Research progress of large field-of-view microsphere lens super-resolution microscopic imaging technology. Infrared and Laser Engineering, 2022, 51(6): 20210438.
[8] McCloskey D, Wang J J, Donegan J F. Low divergence photonic nanojets from Si3N4 microdisks. Optics Express, 2012, 20(1): 128-140.
[9] Luk'yanchuk B S, Paniagua-Domínguez R, Minin I V, et al. Refractive index less than two: photonic nanojets yesterday, today and tomorrow [Invited]. Optical Materials Express, 2017, 7(6): 1820-1847.
[10] Minin I V, Minin O V, Geints Y E. Localized EM and photonic jets from non-spherical and non-symmetrical dielectric mesoscale objects: Brief review. ANNALEN DER PHYSIK, 2015, 527: 491-497.
[11] Sun Z, Liu W, Ge S, et al. Study on photonic nanojets based on double-layer micropyramid structure coupled with spatial light modulation. Acta Photonica Sinica, 2022, 51(12): 1223001.
[12] Veluthandath A V, Murugan G S. Photonic Nanojet Generation Using Integrated Silicon Photonic Chip with Hemispherical Structures. Photonics, 2021, 8(12): 586.
[13] Zhen Z, Huang Y, Feng Y, et al. An ultranarrow photonic nanojet formed by an engineered two-layer microcylinder of high refractive-index materials. Optics Express, 2019, 27(6): 9178-9188.
[14] Gu G, Shao L, Song J, et al. Photonic hooks from Janus microcylinders. Optics Express, 2019, 27(26): 37771-37780.
[15] Amann M C, Bosch T, Lescure M, et al. Laser ranging: a critical review of usual techniques for distance measurement. Optical Engineering, 2001, 40(1): 10-19.
[16] Rogalski A. History of infrared detectors. Opto-Electronics Review, 2012, 20(3): 279-308.
[17] Darafsheh A. Photonic nanojets and their applications. Journal of Physics: Photonics, 2021, 3(2): 022001.
[18] Sun Z, et al. Geometry-Dependent Photonic Nanojet Formation and Arrays Coupling. Nanomaterials, 2026, 16(2): 136.
[19] Geints Y E, Zemlyanov A A, Minin I V. Specular-reflection photonic nanojet. Optics Express, 2020, 28(15): 22690-22704.
[20] Yang M, Wang F, Hao X, et al. Super-resolution imaging and fluorescence enhancement based on microsphere modulated optical field. Laser & Optoelectronics Progress, 2023, 60(10): 1000001.
[21] Ren Y X, et al. Photonic Nanojet Mediated Backaction of Dielectric Microparticles. ACS Photonics, 2020, 7(6): 1483-1490.
[22] Itagi A V, Challener W A. Optics of photonic nanojets. Journal of the Optical Society of America A, 2005, 22(12): 2847-2858.
[23] Devilez A, Bonod N, Wenger J, et al. Three-dimensional subwavelength confinement of light with dielectric microspheres. Optics Express, 2009, 17(4): 2089-2094.
[24] Geints Y E, Zemlyanov A A, Panina E K. Photonic nanojet properties of dielectric microparticles. Journal of the Optical Society of America B, 2011, 28(8): 1825-1830.
[25] Sun M, Duan S, Gao D, et al. Research progress on near-field focusing and far-field imaging simulation of microsphere lenses. Infrared and Laser Engineering, 2022, 51(2): 20220086.